SOLUTION RECONSTRUCTION AND LIMITING FOR THE 2D EULER EQUATIONS IN CENTROID-DUAL…

Conference Paper · May 2013

CITATIONS

0

3 authors, including:

Ioannis K Nikolos

Technical University of Crete

96 PUBLICATIONS **904** CITATIONS

SEE PROFILE

Argiris Delis

Technical University of Crete

49 PUBLICATIONS **535** CITATIONS

SEE PROFILE

SOLUTION RECONSTRUCTION AND LIMITING FOR THE 2D EULER EQUATIONS IN CENTROID-DUAL UNSTRUCTURED FINITE VOLUMES

Agoritsa Antoniou[1], Ioannis K. Nikolos[2], and Anargyros I. Delis[3]

[1,2]Department of Production Engineering and Management
Technical University of Crete
Chania, GR-73100, Greece
[3]Department of Sciences, Division of Mathematics
Technical University of Crete
Chania, GR-73100, Greece
[1]e-mail: ritsaantoniou@hotmail.com
[2]e-mail: jnikolo@dpem.tuc.gr
[3]e-mail: adelis@science.tuc.gr

Keywords: Compressible flows, Euler equations, unstructured grids, solution reconstruction, multidimensional-type limiting procedures

Abstract. *Various solution reconstruction and limiting strategies have been proposed so far for multidimensional Finite Volume (FV) schemes on unstructured meshes as to achieve high order accuracy. This work extends the application of a multidimensional-type solution reconstruction and limiting procedure into the discretization of the 2D Euler equations in centroid-dual finite volumes. This procedure is based on a MUSCL-type technique, but takes into account the geometrical characteristics of the unstructured finite volumes, having as a result to cure potential loss of accuracy from poorly connected grids. The procedure can be implemented in various types of unstructured and hybrid grids, both cell-centered and node-centered ones, while it is independent of the Riemann solver used. In this work, the methodology is developed for centroid-dual volumes, produced by connecting the centroids of adjacent elements with straight lines. A compatible to the reconstruction procedure limiting strategy is proposed as to retain the monotonicity in the solution by utilizing different edge-based limiters. Standard test cases are used to assess the performance of the proposed reconstruction in retaining the formal order of accuracy, and capturing key features of the flows. The compatibility of various types of edge-based limiters with the proposed technique is also discussed.*

1 INTRODUCTION

The design of accurate, robust and efficient methods for numerically solving hyperbolic conservation laws is a very active area in computational fluid dynamics (CFD). Though most of the mathematical theory for Euler and Navier-Stokes equations is developed in simple one-dimensional space, it is readily extended to analyzing multi-dimensional flow and solving the flow pattern around intricate boundaries. As a consequence, intense research has been carried out to handle complex geometries. The development of unstructured mesh finite volume (FV) techniques is one on the most successful approaches, due to its flexible tessellation and conservation properties. Along with automatic and fast mesh generation, a robust high-resolution FV scheme (usually based on higher-order accurate reconstructions) is also essential to capture complex flow structures with an adequate number of grid points, without producing non-physical oscillations near discontinuities such as shock waves. Spurious oscillations may lead to wrong solutions as well as serious convergence problems. Therefore, a robust and accurate oscillation control strategy should be incorporated into a higher order interpolation scheme. Many methodologies to control numerical oscillations have been developed (especially on structured meshes), and several limiting concepts have been proposed, with the most known and successful ones being the TVD, TVB and ENO/WENO ones. However, directly adapting these strategies to, different type of, unstructured meshes it is often insufficient for multidimensional flows, with the main difficulty with unstructured meshes being the translation of directionality and cell neighbor information of proven structured methods. Thus, the search for efficient reconstruction and limiting processes, in a multidimensional context, is still an active field of research, see for example [1, 2, 3] and references therein. Recently[4,5], a cell-centered FV scheme of the Godunov-type with a novel MUSCL-type solution reconstruction and limiting procedure was developed and tested for shallow water flow computations. This novel alternative procedure was developed in order to apply in the reconstruction an edge-based limiting strategy that takes into account geometrical characteristics of the computational mesh. The use of edge-type limiters avoids the procedure of solving any minimization problems or the need to use any tunable parameters. Grids with poor connectivity[6, 5], i.e. those whose flux integration points do not coincide with the location to which reconstructed values are computed, can

be properly treated.

The aim of the present paper is to extend the application and development of this new solution reconstruction and limiting strategy to the approximation of the two-dimensional Euler equations in centroid-dual finite volumes, as to effectively simulate complex compressible flows, and to verify our claim that the procedure can be implemented in various types of unstructured and hybrid grids, both of the cell-centered and node-centered type, while it is independent of the Riemann solver used. To this end, two well-known approximate Riemann solvers are implemented here, demonstrating the procedure's independence to the solver used. In addition, various edge-based limiter functions are tested and comparisons with a cell-centered FV scheme that adopts the same procedure are also presented.

2 THE EULER EQUATIONS AND THE FINITE VOLUME FRAMEWORK

The 2D Euler equations are written in conservative form as

$$\partial_t \mathbf{U} + \nabla \cdot \mathcal{H}(\mathbf{U}) = 0 \quad \text{on} \quad \Omega \times [0,t] \subset \mathbb{R}^2 \times \mathbb{R}^+ \tag{1}$$

where $\mathbf{U}$ is the vector of the conserved variables, $\mathcal{H} = [\mathbf{F}, \mathbf{G}]$ are the nonlinear flux vectors and $\Omega \times [0,t]$ is the space-time Cartesian domain. The conserved variables vector and the flux vectors are defined as

$$\mathbf{U} = \begin{bmatrix} \rho \\ \rho u \\ \rho v \\ \rho e_T \end{bmatrix}, \quad \mathbf{F}(\mathbf{U}) = \begin{bmatrix} \rho u \\ \rho u^2 + p \\ \rho uv \\ (\rho e_T + p)u \end{bmatrix}, \quad \mathbf{G}(\mathbf{U}) = \begin{bmatrix} \rho v \\ \rho uv \\ \rho v^2 + p \\ (\rho e_T + p)v \end{bmatrix} \tag{2}$$

where ρ is the density of the flow, p is the pressure, e_T is the specific total energy, and $\mathbf{u} = [u,v]^T$ is the velocity vector. The state of the perfect gas is used to close the system

$$p = (\gamma_s - 1)(\rho e_T - \frac{1}{2}\rho \|\mathbf{u}\|^2) \tag{3}$$

where γ_s=1.4 is the ratio of the specific heats. Appropriate initial and boundary conditions should be used to close the hyperbolic system of equations, according to the problem under consideration.

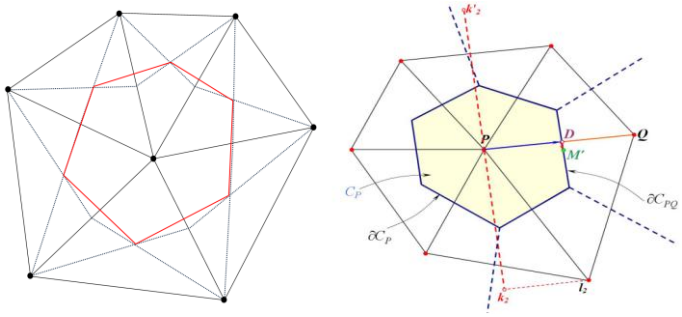

Figure 1. (Left) The construction of the centroid-dual control volume. (Right) The modified reconstruction procedure

For the discretization of the hyperbolic system (1) we utilize the partitioning of the computational domain Ω into a set of non-overlapping control volumes, to be used for the integration of (1). For the centroid-dual Node-Centered Finite Volume (NCFV) scheme considered in this work, a conforming triangulation of Ω is initially performed and the control volumes result by connecting the centroids of adjacent triangular elements with straight line segments; solution values are defined at the nodes of the initial triangular mesh (Figure 1).

To perform convergence studies the major requirement for a sequence of refined grids is to satisfy the *consistency refinement property*[7], which requires that the maximum distance across the control volumes to decrease consistently with increase of the total number of data points *N*. For a given computational domain $L_x \times L_y$ we define a subdivision of L_x by N_x: $\Delta x = L_x/N_x$. The characteristic length h_N of the control volumes is then defined as $h_N = \sqrt{(L_x \times L_y)/N}$, and for a consistently refined grid we have to half Δx, and subsequently $h'_N \simeq h_N / 2$ while $N' \simeq 4N$.

The integral form of equation (1) over a general control volume C_P around node P is given as:

$$\frac{\partial}{\partial t}\iint_{C_P}\mathbf{U}\,dxdy+\iint_{C_P}(\nabla\cdot\mathcal{H})\,dxdy=0 \tag{4}$$

By applying the Gauss' divergence theorem to the flux integral leads to

$$\frac{\partial}{\partial t}\iint_{C_P}\mathbf{U}\,dxdy+\oint_{\partial C_P}\mathcal{H}\cdot\mathbf{n}\;\,dl=0 \tag{5}$$

where ∂C_P is the boundary of the control volume C_p and $\mathbf{n}$ is the unit outward normal vector to the control volume. By denoting as $\mathbf{U}_P$ the average value of the conserved quantities over the volume at a given time, the following conservation equation is written for each cell:

$$\frac{\partial\mathbf{U}_P}{\partial t}=-\frac{1}{|C_P|}\oint_{\partial C_P}\mathbf{F}n_x+\mathbf{G}n_y\;\,dl \tag{6}$$

The Jacobian matrix $\mathbf{J}$ of the normal flux $\mathcal{H}\cdot\mathbf{n}$ is given as $\mathbf{J}=\dfrac{\partial\;\mathcal{H}\cdot\mathbf{n}}{\partial\mathbf{U}}=\left(\dfrac{\partial\mathbf{F}}{\partial\mathbf{U}}n_x+\dfrac{\partial\mathbf{G}}{\partial\mathbf{U}}n_y\right)$.

With ∂C_{PQ} we define the common part of ∂C_P and ∂C_Q, the outward normal vector to ∂C_{PQ} being $\mathbf{n}_{PQ}=[n_{PQx},n_{PQy}]^{\mathrm{T}}$, while $\mathbf{n}_{PQ}=[n_{PQx},n_{PQy}]^{\mathrm{T}}$ is the corresponding unitary one; then $\mathbf{n}_{PQ}=\int_{\partial C_{PQ}}\mathbf{n}\,dl$. If Γ is the domain's boundary and K_P is the set of neighboring nodes to P, then ∂C_P is described as:

$$\partial C_P=\bigcup_{Q\in K_P}\partial C_{PQ}+(\partial C_P\cap\Gamma) \tag{7}$$

By introducing the flux vectors $\mathbf{\Phi}_{PQ}=\int_{\partial C_{PQ}}(\mathbf{F}n_x+\mathbf{G}n_y)dl$ and $\mathbf{\Phi}_{P,out}=\int_{\partial C_P\cap\Gamma}(\mathbf{F}n_x+\mathbf{G}n_y)dl$ equation (6) becomes:

$$\frac{\partial\mathbf{U}_P}{\partial t}|C_P|+\sum_{Q\in K_P}\mathbf{\Phi}_{PQ}+\mathbf{\Phi}_{P,out}=0 \tag{8}$$

For all volume faces the flux vector $\mathbf{\Phi}_{PQ}$ should be evaluated and added with the proper sign to the flux sum of the two adjacent cells C_P and C_Q. Assuming a linear distribution of $\mathcal{H}$ over ∂C_P, this flux is computed by its value at the midpoint M' of the volume face that corresponds to edge PQ (Figure 1(Right)):

$$\mathbf{\Phi}_{PQ}=\int_{\partial C_{PQ}}(\mathbf{F}n_x+\mathbf{G}n_y)dl\approx(\mathbf{F}n_x+\mathbf{G}n_y)_{M'}\left\|\mathbf{n}_{PQ}\right\|=(\mathbf{F}n_{PQx}+\mathbf{G}n_{PQy})_{M'} \tag{9}$$

In order to evaluate this flux at M' a one dimensional Riemann problem is assumed between the left (L) and the right (R) states at the two sides of M', solved using the Roe's[8, 9] or the HLLC[9] approximate Riemann solvers. A first order scheme results if the left and right states at point M' are approximated with the values at points P and Q respectively.

3 SECOND-ORDER SCHEME

Our second-order scheme is based on a MUSCL-type[10] reconstruction of the primitive variables, although the proposed ideas can be applied to conservative and characteristic ones (assuming that the solution varies linearly in each control volume). Slope limiting is used to control the total variation of the reconstructed variables. Strict monotonicity in the reconstruction of the primitive variables is enforced by the use of edge-based limiter functions, usually reserved for node-centered FV schemes of the median-dual type. The standard limiter used here is the modified Van Albada-Van Leer limiter [11], being differentiable for linearly varying flow variables.

Since we wish to apply edge-based limiters, we have to initially compute reconstructed values at the intersection point D of edge $\overline{PQ}$ and face ∂C_{PQ} (Figure 1(Right)), in order to be able to compare with the reference value $(\mathrm{w}_{i,Q}-\mathrm{w}_{i,P})$ of the primitive variables at nodes P and Q. The left and right extrapolated values at point D are then computed as:

$$(\mathrm{w}_{i,P})_D^L = \mathrm{w}_{i,P} + \mathbf{r}_{PD} \cdot \nabla \mathrm{w}_{i,P}, \ (\mathrm{w}_{i,Q})_D^R = \mathrm{w}_{i,Q} - \mathbf{r}_{DQ} \cdot \nabla \mathrm{w}_{i,Q}, \tag{10}$$

In general point *D* does not coincide with the midpoint *M'* of the face ∂C_{PQ}. In order to apply a limiter function, its arguments (being consecutive gradients of the solution) should be defined around face ∂C_{PQ}. We define a virtual point *Q'* being upwind of *Q* (Figure 1(Right)). By denoting as $(\nabla \mathrm{w}_{i,Q})^{cnt} \cdot \mathbf{r}_{PQ} = (\mathrm{w}_{i,Q} - \mathrm{w}_{i,P})$ we compute the upwind gradient $(\mathrm{w}_{i,Q} - \mathrm{w}_{i,Q'})$ by assuming that point *Q'* lies along $\overline{PQ}$ and *Q* is the midpoint of $\overline{PQ}'$. Then:

$$\begin{aligned} &\mathrm{w}_{i,Q'} - \mathrm{w}_{i,Q} = (\mathrm{w}_{i,Q'} - \mathrm{w}_{i,P}) - (\mathrm{w}_{i,Q} - \mathrm{w}_{i,P}) = (\nabla \mathrm{w}_{i,Q}) \cdot \mathbf{r}_{PQ'} - (\mathrm{w}_{i,Q} - \mathrm{w}_{i,P}) \\ &= 2(\nabla \mathrm{w}_{i,Q}) \cdot \mathbf{r}_{PQ} - (\nabla \mathrm{w}_{i,Q})^{cnt} \cdot \mathbf{r}_{PQ} \end{aligned} \tag{11}$$

As point *D* does not coincide in general with the middle of edge $\overline{PQ}$ limiting should take into account the ratio of the corresponding lengths:

$$\begin{aligned} (\mathrm{w}_{i,Q})_D^R &= \mathrm{w}_{i,Q} - \frac{\|\mathbf{r}_{DQ}\|}{\|\mathbf{r}_{PQ}\|} \mathrm{F}_{\mathrm{LIM}}((\nabla \mathrm{w}_{i,Q})^{upw} \cdot \mathbf{r}_{PQ}, (\nabla \mathrm{w}_{i,Q})^{cnt} \cdot \mathbf{r}_{PQ}) \\ (\mathrm{w}_{i,P})_D^L &= \mathrm{w}_{i,P} + \frac{\|\mathbf{r}_{PD}\|}{\|\mathbf{r}_{PQ}\|} \mathrm{F}_{\mathrm{LIM}}((\nabla \mathrm{w}_{i,P})^{upw} \cdot \mathbf{r}_{PQ}, (\nabla \mathrm{w}_{i,P})^{cnt} \cdot \mathbf{r}_{PQ}) \end{aligned} \tag{12}$$

The upwind limiter arguments above are defined as:

$$(\nabla \mathrm{w}_{i,Q})^{upw} = 2\nabla \mathrm{w}_{i,Q} - (\nabla \mathrm{w}_{i,Q})^{cnt}, \ (\nabla \mathrm{w}_{i,P})^{upw} = 2\nabla \mathrm{w}_{i,P} - (\nabla \mathrm{w}_{i,P})^{cnt} \tag{13}$$

As point *D* does not coincide in general with the middle *M'* of the face ∂C_{PQ}, for grids where the distance between those points is large, the interpolation is expected to be only first-order accurate. For the correction of this inconsistency a procedure was proposed [5] and a directional correction is applied to the values at *D* in order to compute the values at *M'*:

$$(\mathrm{w}_{i,P})_{M'}^L = (\mathrm{w}_{i,P})_D^L + \mathbf{r}_{DM'} \cdot \nabla \mathrm{w}_{i,P}, \ \ (\mathrm{w}_{i,Q})_{M'}^R = (\mathrm{w}_{i,Q})_D^R + \mathbf{r}_{DM'} \cdot \nabla \mathrm{w}_{i,Q} \tag{14}$$

This (unlimited) modification retains second order accuracy for smooth flows, even for highly stretched meshes and such ones with large distances between points *D* and *M'* (tested for cell-centered grids for the solution of the shallow water equations[5]). In order to correctly solve flows where shocks are present, the unlimited terms in the equations above should be properly limited along $\overline{DM}'$. For doing this (for the left part of the reconstruction on the corresponding face), we have to identify the set of nodes l_j, *j*=1,2,... of the triangles that share *P* as a common vertex and lie in the direction of $\overline{DM}'$. The reference node to be selected is the one for which $\overline{Pl_j}$ has the smallest angle with $\overline{DM}'$ (l_2 in Figure 1(Right)). We then project this node in the direction of $\overline{DM}'$ taking $\overline{Pk_2}$. The extrapolated primitive value at k_2 is computed using the relevant value at l_2 as:

$$\mathrm{w}_{i,k_2} = \mathrm{w}_{i,l_2} + \mathbf{r}_{l_2 k_2} \cdot \nabla \mathrm{w}_{i,l_2} \tag{15}$$

Then, the local central reference gradient can be defined as $(\nabla \mathrm{w}_{i,P})^{cnt} \cdot \mathbf{r}_{Pk_2} = (\mathrm{w}_{i,k_2} - \mathrm{w}_{i,P})$, while the corresponding upwind gradient $(\mathrm{w}_{i,P} - \mathrm{w}_{i,k'_2})$ can be defined by introducing the virtual node k'_2 and following the previously described procedure (Figure 1(Right)). Then, the limited values of the primitive quantities at *M'* can be evaluated as:

$$\begin{aligned} &(\mathrm{w}_{i,P})_{M'}^L = (\mathrm{w}_{i,P})_D^L + \frac{\|\mathbf{r}_{DM'}\|}{\|\mathbf{r}_{Pk_2}\|} \mathrm{F}_{\mathrm{LIM}}((\nabla \mathrm{w}_{i,P})^{upw} \cdot \mathbf{r}_{Pk_2}, (\nabla \mathrm{w}_{i,P})^{cnt} \cdot \mathbf{r}_{Pk_2}) \\ &(\nabla \mathrm{w}_{i,P})^{upw} = 2\nabla \mathrm{w}_{i,P} - (\nabla \mathrm{w}_{i,P})^{cnt} \end{aligned} \tag{16}$$

Using a similar procedure, the right limited reconstructed values at M' can be computed as well. The Green-Gauss procedure is used to compute the gradients in each computational cell. The time integration is performed using a second-order explicit Runge-Kutta scheme[5], while the time step computation is based on the usual CFL stability condition.

Grid Type						
	Type I and IV		***Type II***		***Type III***	
N_x	N	h_N	N	h_N	N	h_N
20	562	0.843649081	841	0.689655172	441	0.952380952
40	1950	0.452910813	3281	0.349161926	1681	0.487804878
80	7579	0.229733348	12961	0.175675314	6561	0.24691358
160	29877	0.115707497	51521	0.088112566	25921	0.124223602
321	119647	0.057820133	205441	0.044125174	103041	0.062305295

Table 1 : Number of data points N, and characteristic length h_N for the consistently refined grids used

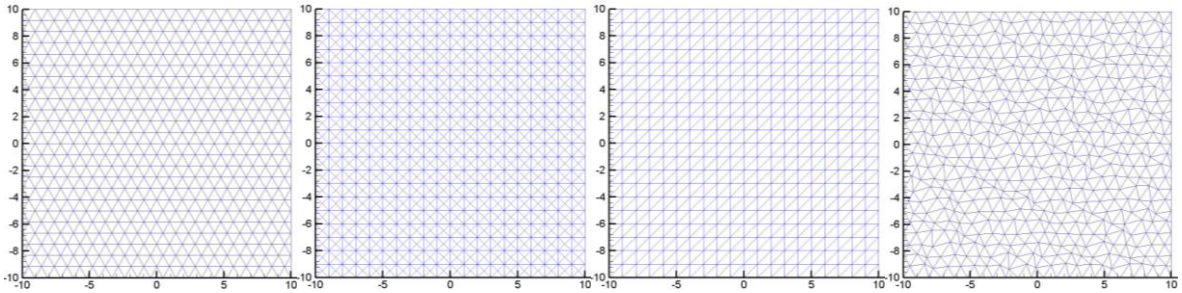

Figure 2. Grid Types I-IV from left to right

4 NUMERICAL RESULTS

4.1 Isentropic Vortex Problem

For this benchmark test problem the exact (smooth) solution is known. The mean flow is computed in a domain Ω=[-10,10]x[-10,10] with periodic boundary conditions in all 4 walls of the domain, with $\rho_\infty = 1,\ p_\infty = 1,\ [u_\infty, v_\infty]^T = [1,1]^T$.

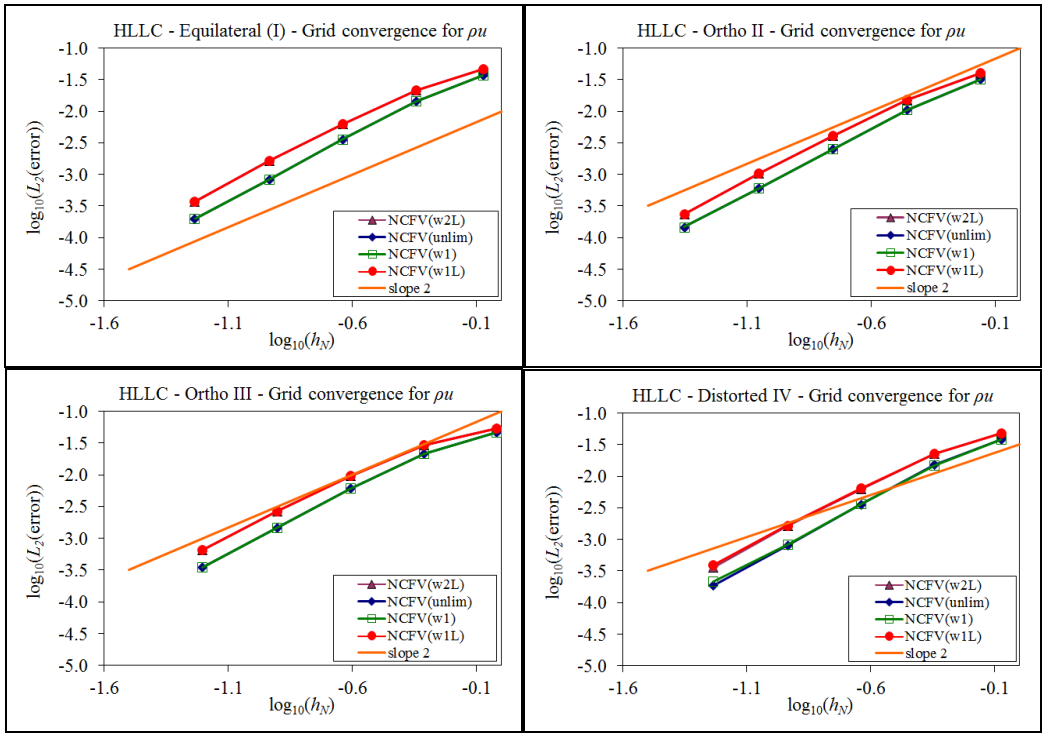

Figure 3. Isentropic vortex: convergence results on all grid types using the HLLC approximate Riemann solver (from left to right, top to bottom): (i) *Type I*, (ii) *Type II*, (iii) *Type III*, (iv) *Type IV*

An isentropic vortex is added to this flow field, initially at point [0,0], and the exact solution in each time step[3, 2] results from the initial solution shifted by $(u_\infty t, v_\infty t)$. By comparing the numerical solution with the exact one at t=2s, we can compute the numerical (dispersion and dissipation) errors of the numerical procedure. Four types of regular and irregular grids are used (Figure 2, Table 1) to test the performance and convergence behavior of the proposed methodology, which are consistently refined as previously described.

Two different approximate Riemann solvers were used (Roe's and HLLC) while the limiting is based on the Van Albada - Van Leer (VA) edge-based limiter, adapted in the prescribed reconstruction procedure. Four different types of reconstruction and limiting were tested: (i) *Unlimited* 2nd order reconstruction at point *M'*, (ii) *W1*: unlimited reconstruction at point *D*, (iii) *W1L*: limited reconstruction at point *D*, (iv) *W2L*: Limited reconstruction at point *M'*. Figure 3 contains convergence results for ρu on all grid types using the HLLC approximate Riemann solver and the four different schemes. Similar results have been obtained using the Roe's approximate Riemann solver, and for all the conserved variables. For all the grid types used the proposed formulation provides a higher than 2nd order rate of convergence, regardless of the fact that the grids exhibit different distances between points *D* and *M'*. The introduction of limiting increases the error of the numerical solution without reducing the rate of convergence.

Figure 4 contains converge rate comparisons of the centroid-dual node-centered *W2L* scheme and the corresponding cell-centered (CC) one, which uses the same procedure for the reconstruction and limiting as the centroid-dual node-centered one[5]. The node-centered scheme shows a small degradation in the convergence rate, compared to the CC one. This is attributed to the fact the CC scheme uses a denser stencil for the gradient computation, which takes into account all the triangles having at least a common node with the current (control volume) triangle.

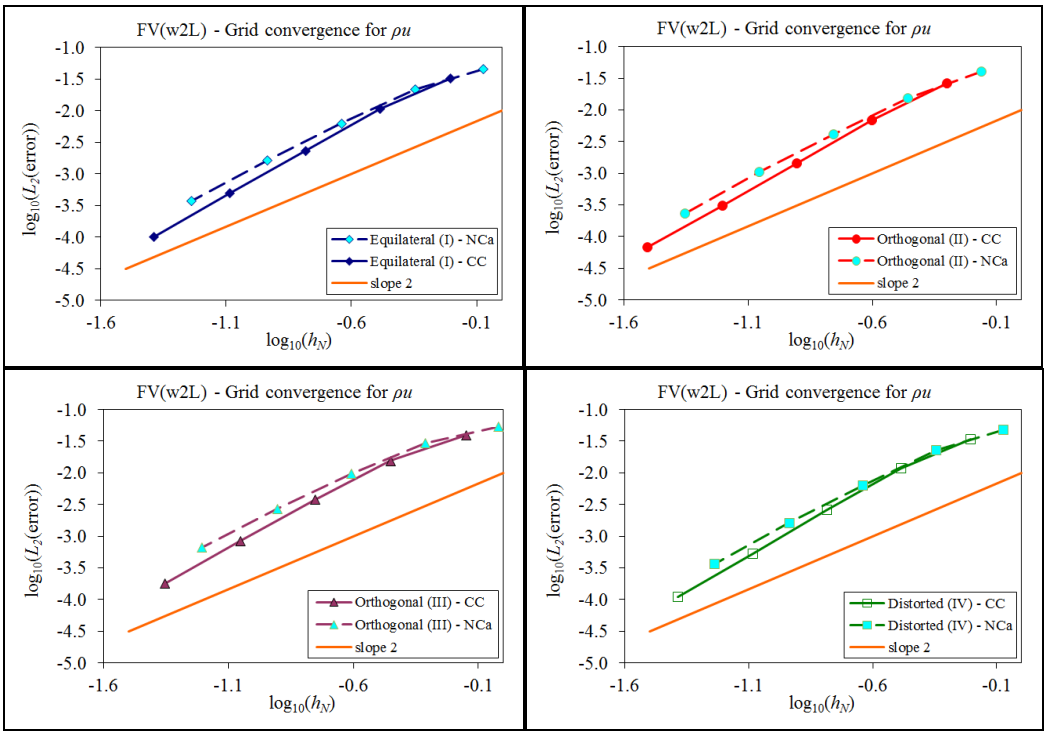

Figure 4. Isentropic vortex: convergence results on all grid types using the Roe's approximate Riemann solver and comparison between the cell-centered (CC) and the centroid-dual node-centered (NCa) approach.

4.2 Transonic flow around NACA0012 airfoil

For this benchmark test case the transonic flow around NACA0012 airfoil is computed at three different flow conditions: (i) *Mach*=0.8, *a*=1.25°, (ii) *Mach*=0.85, *a*=1.0°, (ii) *Mach*=2.0, *a*=0.0°. The grid consists of 6492 triangular elements and 3366 nodes (data points) with 200 nodes on the airfoil (Figure 5). Two different approximate Riemann solvers were used (Roe's and HLLC) and five different edge-based limiting functions[5]: (i) Van Albada - Van Leer (VA), (ii) Min-mod (MM), (iii) SuperBee (SB), (iv) MC, (v) Van Leer (VL), all combined with the prescribed reconstructing and limiting procedure (*W2L*). Here we present computation results only for the Mach=0.8 and Mach=2.0 cases (using HLLC), for brevity reasons. Figure 6 contains convergence histories for the different edge-based limiters and the corresponding *Cp* diagrams for the *Mach*=0.8 case; Mach

number contours using the MM limiter and the *W2L* reconstruction scheme are also presented. The convergence histories demonstrate that the *W2L* scheme coupled with the SB and the MC edge-based limiters failed to achieve an acceptable convergence. Such very sharp limiters are not a favorable selection for coupling with the proposed reconstruction and limiting procedure, while smother limiters seem to be a better choice. These conclusions are supported by the *Cp* diagrams in Figure 6, where for the two afore-mentioned limiters oscillations start to appear at the regions of the shock discontinuities. Mach number contours produced using the MM limiter and the *W2L* scheme are also presented in Figure 6. Figure 7 contains the convergence histories and the *Cp* diagrams for the *Mach*=2.0 case. For the SB limiter the scheme failed to converge, while for the VA limiter the convergence of the continuity residual stops at about 10^{-12}. Mach number contours close to the leading edge of the airfoil are also presented in Figure 7 for the SB, MM, and VA limiters. Large oscillations are observed for the SB limiter (which has not converged), and smaller ones for the VA one.

The results also support the previous conclusion that the proposed reconstruction procedure should be combined with smooth edge-based limiters. Nevertheless, this work demonstrated that the proposed reconstruction and limiting procedure, that takes into consideration the geometrical characteristics of the unstructured mesh, can be effectively applied for the solution of different hyperbolic type problems, (with cell-centered or centroid-dual node centered formulations), combined with different Riemann solvers and edge based limiters.

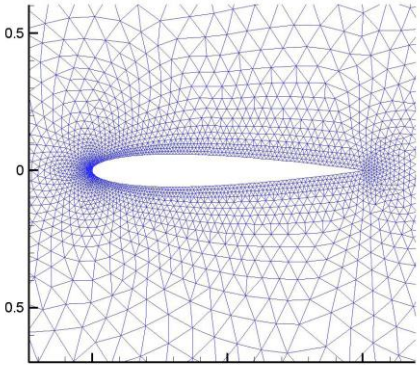

Figure 5. NACA0012: The unstructured triangular grid close to the airfoil

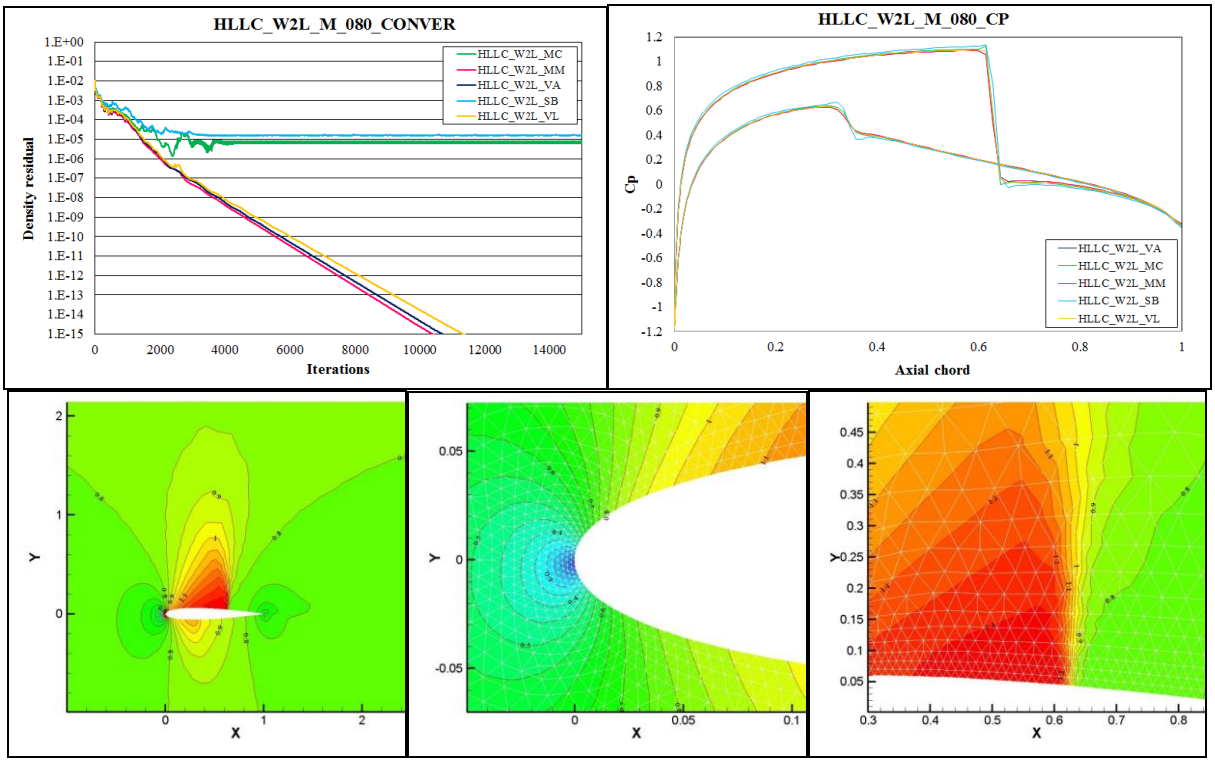

Figure 6. NACA0012, *Mach*=0.8, *a*=1.25°, HLLC, *W2L*: (Top left) continuity residual convergence histories for the different edge-based limiters; (Top right) *Cp* diagrams for the different edge-based limiters; (Bottom) Mach number contours using the MM limiter and the *W2L* reconstruction scheme

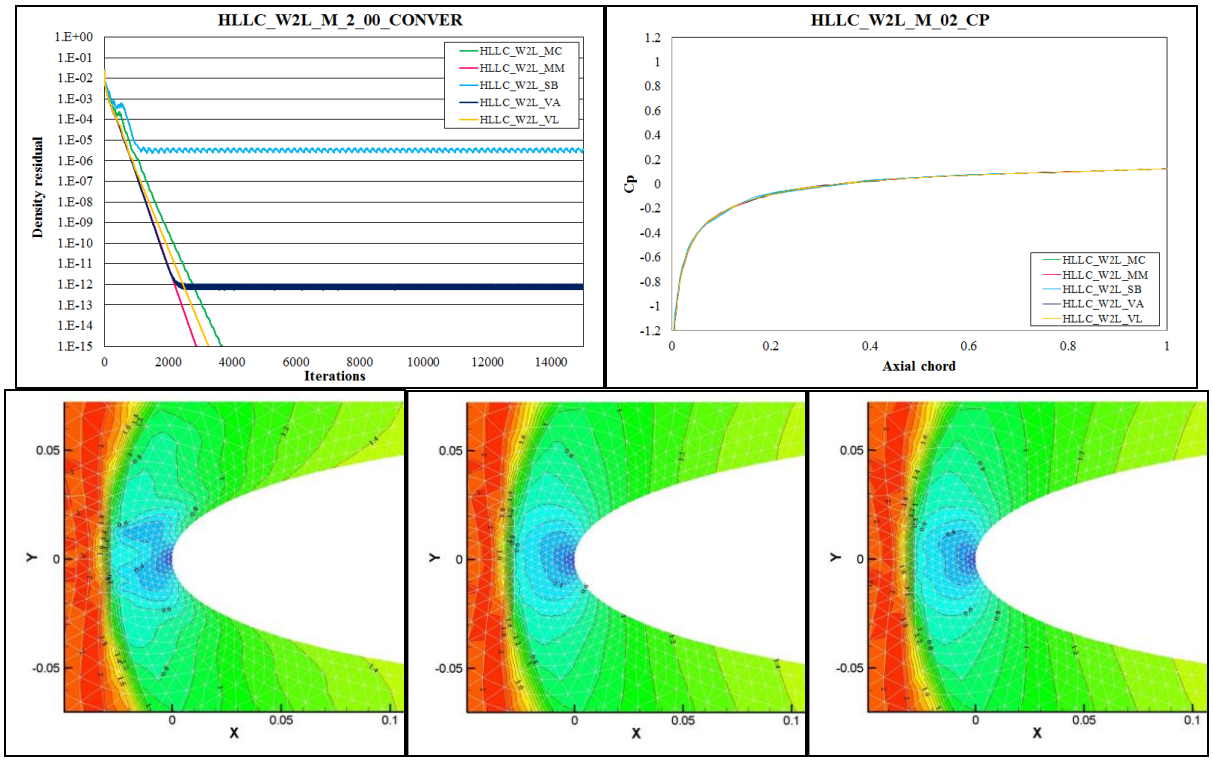

Figure 6. NACA0012, Mach=2.0, a=0.0^{o}, HLLC, *W2L*: (Top left) continuity residual convergence histories for the different edge-based limiters; (Top right) *Cp* diagrams for the different edge-based limiters; (Bottom) Mach number contours near the leading edge using the SB (left), MM (center), and VA (right) limiters with the *W2L* reconstruction scheme

REFERENCES

[1] Clain, S. and Clauzon, V. (2010), "Monoslope and multislope MUSCL methods for unstructured meshes", *Journal of Computational Physics*, 229, pp. 3745-3776.

[2] Li, W., Ren, Y.-X., Lei, G., and Luo, H. (2011), "The multi-dimensional limiters for solving hyperbolic conservation laws on unstructured grids", *Journal of Computational Physics*, 230, pp. 7775-7795.

[3] Park, J.S., Yoon, S.-H., and Kim, C. (2010), "Multi-dimensional limiting process for hyperbolic conservation laws on unstructured grids", *Journal of Computational Physics*, 229, pp. 788-812.

[4] Delis, A.I., Nikolos, I.K., and Kazolea, M. (2011), "Performance and comparison of cell-centered and node centered unstructured finite volume discretizations for shallow water free surface flows", *Archives of Computational Methods in Engineering*, 18, pp. 57-108.

[5] Delis, A.I. and Nikolos, I.K. (2013), "A novel multi-dimensional solution reconstruction and edge-based limiting procedure for unstructured cell-centered finite volumes with application to shallow water dynamics", *International Journal for Numerical Methods in Fluids*, 71(5), pp. 584-633.

[6] Hubbard, M.E. (1999), "Multi-dimensional slope limiters for MUSCL-type finite volume schemes on unstructured grids", *Journal of Computational Physics*, 155, pp. 54-74.

[7] Diskin, B., Thomas, J.L. (2010), "Comparison of node-centered and cell-centered unstructured finite volume discretizations: inviscid fluxes", *48th AIAA Aerospace sciences meeting including the New Horizons Forum and Aerospace Exposition*, Orlando, Florida, AIAA paper 2010-1079.

[8] Roe, P.L. (1981), "Approximate Riemann solvers, parameter vectors, and difference schemes", *Journal of Computational Physics*, 43, pp. 357-372.

[9] Toro, E.F. (1997), *Riemann solvers and numerical methods for fluid dynamics*, Springer, Berlin.

[10] Van Leer, B. (1979), "Towards the ultimate conservative difference scheme V. A second order sequel to Godunov's method", *Journal of Computational Physics*, 32, pp. 101-136.

[11] Van Albada, G.D., Van Leer, B., Roberts, W.W. (1982), "A comparative study of computational methods in cosmic gas dynamics", *Astronomy and Astrophysics*, 108, pp. 46–84.